Journal of Hydraulic Research Vol. 47, No. 6 (2009), pp. 764–776
doi:10.3826/jhr.2009.3438

Verification of Q-QUICK scheme for convective flux in incompressible flow on unstructured grids

Vérification du schéma Q-QUICK sur des grilles non structurées pour les flux convectifs dans un écoulement incompressible

ZULIN HUA, *Key Laboratory of Integrated Regulation and Resource Development on Shallow Lake of Ministry of Education, College of Environmental Science and Engineering, Hohai University, Nanjing 210098, China. E-mail: zulinhua@hhu.edu.cn*

LINGHANG XING, *Yangtze River Scientific Research Institute, Wuhan 430010, China. E-mail: xinglinghang@sina.com*

KEJIAN CHU, *Key Laboratory of Integrated Regulation and Resource Development on Shallow Lake of Ministry of Education, College of Environmental Science and Engineering, Hohai University, Nanjing 210098, China. E-mail: kejianc@hhu.edu.cn (author for correspondence)*

LI GU, *State Key Laboratory of Hydrology-Water Resources and Hydraulic Engineering, Hohai University, Nanjing 210098, China. E-mail: guliqc@hhu.edu.cn*

ABSTRACT
Accuracy of convective flux approximation is important for numerical computation of incompressible flow on unstructured grids. The Quasi-QUICK scheme by Davidson is proposed to improve the accuracy of convective flux approximation. The numerical performances of the Q-QUICK scheme on unstructured grids are explored, including numerical accuracy, convergence stability, CPU time consumption and solution sensitivity to high grid deformation. Several test cases such as 90° and 30° 2D lid-driven cavity flows, diverging channel and 3D lid-driven cavity flow are considered. The results show that the Q-QUICK scheme performs well in terms of numerical accuracy, convergence stability or adaptability to high grid deformation if compared with other schemes. Moreover, the convergence speed of momentum equation and CPU time consumptions are also compared for each type of grid and scheme.

RÉSUMÉ
La précision de l'approximation du flux convectif est importante pour le calcul numérique des écoulements incompressibles sur les grilles non structurées. Le schéma Quasi-QUICK de Davidson est proposé pour améliorer la précision de l'approximation du flux convectif. Les performances numériques du schéma Q-QUICK sur les grilles non structurées sont étudiées, y compris la précision numérique, la stabilité de convergence, la consommation de temps CPU et la sensibilité de la solution aux fortes déformations de grille. Plusieurs cas tests sont considérés comme les écoulements 2D en cavité pilotés par couvercle à 90° et 30°, un canal divergent et l'écoulement 3D en cavité piloté par couvercle. Les résultats montrent que le schéma Q-QUICK a de bonnes performances en termes de précision numérique, de stabilité de la convergence ou d'adaptabilité à une forte déformation de grille si on le compare aux autres schémas. En outre, la rapidité de convergence de l'équation des quantités de mouvement et les consommations de temps CPU sont également comparées pour chaque type de grille et de schéma.

Keywords: Convective flux, Incompressible flow, Numerical computation, Q-QUICK, Unstructured grid

1 Introduction

In numerical simulation of incompressible flow, unstructured grids can well fit to complex physical boundaries for both 2D or 3D flows. Thus a computation based on unstructured grids becomes more and more prevalent. However, many numerical schemes on structured grids can not be directly applied to unstructured grids. It is imperative to study high-precision schemes that fit to the computation on unstructured grids, in particular for coarse grids.

In the past decades, a number of difference schemes to calculate convective flux were developed for incompressible flow simulation. They include the Upwind Difference Scheme (UDS), Central Differencing Scheme (CDS), Hybrid Differencing Scheme (HDS), Quadratic Upstream Interpolation for Convective Kinematics scheme (QUICK) (Leonard 1979), Quadratic

Revision received July 6, 2009/Open for discussion until June 30, 2010.

Upstream Extended and Quadratic Upstream Extended Revised Difference Scheme (QUDSE, QUDSER as modified by Pollard and Siu 1982), the Locally Exact Difference Scheme (LEDS) (Spalding 1972) and the Power Difference Scheme (PDS) (Pantankar 1980). The unconditionally-convergent schemes UDS/HDS/LEDS/PDS may become highly inaccurate on coarse grids. Thus, they require considerable grid refinement to produce acceptable results, rendering them costly (Patel and Markatos 1986). Moreover, they implicitly introduce the numerical diffusion term and distort the solution. In terms of accuracy and computational efficiency, it appears that QUICK/QUDSE/QUDSER may offer the best compromise (e.g. Patel and Markatos 1986). For uniform grids, they can have high-order accuracy for incompressible convective flux approximation and are widely applied (e.g. Berour *et al*. 2007, Carvalho *et al*. 2008, Wei *et al*. 2002, Stamou *et al*. 2008). However, QUICK/QUDSE/ QUDSER need the nodes of two upstream cells. Then it is not so easy to apply these high-order schemes to unstructured grids directly, especially in three-dimensional (3D) problems. Moreover, searching for the exact locations of the far-upstream nodes on unstructured grids increases computational complexity, and consumes more memory and CPU time. Furthermore, for multi-dimensional flows involving three or more sets of equations, the computation capacity of current computers still proves to be the limiting factor in the use of very fine grids. Therefore, high-order interpolation schemes of sufficient accuracy are required to permit the performance of complex computations on relatively coarse grids.

Davidson (1996) introduced Quasi-QUICK (Q-QUICK) in which the far-upstream node is constructed by intersection from the line of two adjacent central points and its corresponding interface. Herein the numerical performances of the Q-QUICK scheme are explored, and several test cases are demonstrated to study its numerical accuracy, convergence stability, CPU time consumption and solution sensitivity to high grid deformation.

2 Governing equations

The governing non-dimensional equations of steady, incompressible flow are

$$\nabla \cdot \vec{u} = 0 \tag{1}$$

$$\vec{u} \cdot \nabla \vec{u} = -\nabla p + \nabla \cdot \left(\frac{1}{\mathsf{R}} \nabla \vec{u} \right) \tag{2}$$

where $\vec{u}$ = velocity, p = pressure, and R = Reynolds number. These equations reveal similarity in their structure. If a typical representative variable is denoted by φ, the general form of these equations is

$$\nabla \cdot (\vec{u}\varphi) = \nabla \cdot (\Gamma_\varphi \nabla \varphi) + S_\varphi \tag{3}$$

where S_φ = source term including pressure for the momentum equation, and Γ_φ = diffusivity. The convection and diffusion terms are embedded in divergence form.

3 Numerical discretization

3.1 *Convection fluxes*

The Finite-Volume Method (FVM) is used to discretize the governing equations on unstructured grids. By first integrating over a control volume and then using Gauss's divergence theorem, Eq. (3) can be written as

$$\sum_{\mathrm{f}} F_{\mathrm{f}}^{\mathrm{c}} = \sum_{\mathrm{f}} F_{\mathrm{f}}^{\mathrm{d}} + \int_{\Omega} S_\varphi \mathrm{d}\Omega \tag{4}$$

where $F_{\mathrm{f}}^{\mathrm{c}} = (A\vec{u} \cdot \vec{n})_{\mathrm{f}} \varphi_{\mathrm{f}}$, $F_{\mathrm{f}}^{\mathrm{d}} = (A\Gamma_\varphi \nabla\varphi \cdot \vec{n})_{\mathrm{f}}$ = convection and diffusion fluxes through one internal face f respectively, A = area, $\vec{n}$ = outward-pointing face area vector, Ω = volume of the control cell.

On the non-uniform structured grid shown in Fig. 1, the QUICK scheme at the east cell-face (between P and E) can be written as

$$\begin{aligned} \varphi_{\mathrm{e}} &= \frac{B_1}{B}\varphi_{\mathrm{P}} - \frac{B_2}{B}\varphi_{\mathrm{E}} + \frac{B_3}{B}\varphi_{\mathrm{W}} \quad (u \geq 0); \\ \varphi_{\mathrm{e}} &= \frac{B_1}{B}\varphi_{\mathrm{P}} - \frac{B_2}{B}\varphi_{\mathrm{E}} + \frac{B_3}{B}\varphi_{\mathrm{EE}} \quad (u < 0) \end{aligned} \tag{5}$$

where $B_1 = \delta_2\delta_3(\delta_2 - \delta_3)$, $B_2 = \delta_1\delta_3(\delta_1 + \delta_3)$, $B_3 = \delta_1\delta_2(\delta_1 + \delta_2)$, $B = B_1 - B_2 + B_3$, $\delta_3 = -(\psi_1 + \delta_1)(u \geq 0)$ or $\delta_3 = \psi_2 + \delta_2(u < 0)$, e = midpoint of line $\overline{\mathrm{PE}}$, δ_1, δ_2 = distances between points P and e, e and E, respectively, ψ_1, ψ_2 = distances between points W and P, E and EE, respectively. This is a third-order approximation of the convection term. However, this high-order scheme is not easily applicable to unstructured grids. Searching for the exact locations of these far-upstream nodes EE or WW on an unstructured grid also increases the geometrical complexity and consumes excessive memory and CPU time.

Davidson (1996) introduced the modified Q-QUCIK scheme. Considering Fig. 2, the far-upstream node U is constructed by the intersection of line $\overline{\mathrm{PG}}$ and its corresponding interface f, with J = centre of the interface f. An appropriate way involves reconstruction schemes (Davidson 1996), namely to compute the gradient at node P and use a Taylor expansion to obtain the value at

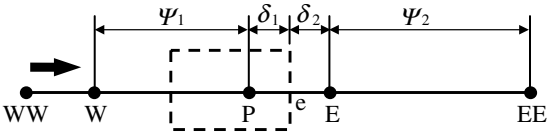

Figure 1 QUICK scheme on non-uniform grid

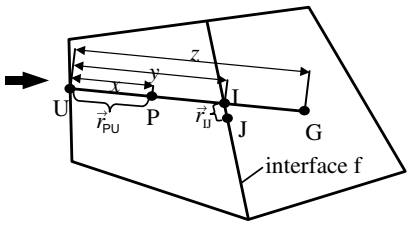

Figure 2 Far-upstream node reconstruction for Q-QUICK convection scheme

node U as

$$\varphi_{\mathrm{U}} = \varphi_{\mathrm{P}} + \vec{r}_{\mathrm{PU}} \cdot (\nabla\varphi)_{\mathrm{P}} + \frac{1}{2}(\vec{r}_{\mathrm{PU}})^2 : (\nabla\nabla\varphi)_{\mathrm{P}} + \cdots + \frac{1}{m!}(\vec{r}_{\mathrm{PU}})^m \underbrace{:::}_{m}(\underbrace{\nabla\nabla\cdots\nabla}_{m}\varphi)_{\mathrm{P}} + \cdots \quad (6)$$

where $\vec{r}_{\mathrm{PU}}$ = distance vector from point P to point U. Herein, a second-order approximation is considered. Thus the first two terms on the right hand side of Eq. (6) are retained. Then, the value at interface f is estimated, by assuming that the flow direction is from left to right. The face value is interpolated by QUICK as for structured grids, resulting for the normal face value φ_{f} in

$$\varphi_{\mathrm{f}} = \varphi_{\mathrm{P}} + (\varphi_{\mathrm{f}})_H \quad (7)$$

where $(\varphi_{\mathrm{f}})_H = f_1\vec{r}_{\mathrm{PU}} \cdot (\nabla\varphi)_{\mathrm{P}} + f_2(\varphi_{\mathrm{G}} - \varphi_{\mathrm{P}}) + \vec{r}_{\mathrm{IJ}} \cdot (\nabla\varphi)_{\mathrm{I}}$, $f_1 = -(z-y)(y-x)x^{-1}z^{-1}$, $f_2 = y(y-x)z^{-1}(z-x)^{-1}$. Then, the convection flux is written as

$$F_{\mathrm{f}}^{\mathrm{c}} = (A\vec{u}\cdot\vec{n})_{\mathrm{f}}\varphi_{\mathrm{P}} + (A\vec{u}\cdot\vec{n})_{\mathrm{f}}(\varphi_{\mathrm{f}})_H \quad (8)$$

During calculation, the upwind flux, i.e. the first term on the right hand side of Eq. (8), is treated implicitly for the merit of diagonal dominance which is beneficial to the solution iteration. The rest of the flux is implemented explicitly and updated after each solution iteration.

3.2 *Diffusion fluxes*

The over-relaxed approach (Jasak 1996, Tsui and Pan 2006, Basara 2004) is used to compute diffusion fluxes due to allow for grid deformation and good numerical stability and accuracy. Its application to approximate diffusion fluxes is governed by

$$F_{\mathrm{f}}^{\mathrm{d}} = (A\Gamma_\varphi)_{\mathrm{f}}\left[|\vec{\Delta}|\frac{\varphi_{\mathrm{G}} - \varphi_{\mathrm{P}}}{d_{\mathrm{PG}}} + (\nabla\varphi)_{\mathrm{f}} \cdot \vec{k}_{\mathrm{f}}\right] \quad (9)$$

where $\vec{\Delta} = \vec{r}_{\mathrm{PG}}/(\vec{r}_{\mathrm{PG}} \cdot \vec{n})$ is parallel to $\vec{r}_{\mathrm{PG}}$, with $\vec{k} = \vec{n} - \vec{\Delta}$ and d_{PG} = distance between P and G. The gradient of variable φ at the interface is obtained via interpolation from values of adjacent cell central nodes with $f_{\mathrm{P}} = |d_{\mathrm{IG}}|/|d_{\mathrm{PG}}|$ as

$$(\nabla\varphi)_{\mathrm{f}} = f_{\mathrm{P}}(\nabla\varphi)_{\mathrm{P}} + (1 - f_{\mathrm{P}})(\nabla\varphi)_{\mathrm{G}} \quad (10)$$

3.3 *Variable gradients*

The gradient of variable φ at point P is approximated by the Gauss theorem

$$(\nabla\varphi)_{\mathrm{P}} = \frac{1}{\Omega}\int_S \varphi\vec{n}\,\mathrm{d}S = \frac{1}{\Omega}\sum_{\mathrm{f}}(A\varphi\vec{n})_{\mathrm{f}} \quad (11)$$

where S = surface of control cell.

3.4 *Discretized momentum equation*

By substituting Eqs. (8), (9) and (11) into Eq. (4), and introducing the under-relaxation coefficient α_φ to further strengthen computational stability results in

$$a_{\mathrm{P}}\frac{\varphi_{\mathrm{P}}}{\alpha_\varphi} - \sum_{\mathrm{f}} a_{nb}\varphi_{nb} = b_{\mathrm{P}} + a_{\mathrm{P}}\frac{(1-\alpha_\varphi)\varphi_{\mathrm{P}}^{\mathrm{o}}}{\alpha_\varphi} \quad (12)$$

where

$$\begin{aligned}
a_{\mathrm{P}} &= \sum_{\mathrm{f}}\{a_{nb} + \max(F_{\mathrm{f}}, 0)\},\\
a_{nb} &= D_{\mathrm{f}}A(|P_{\mathrm{f}}|) + 2(1-\omega_f)\max(-F_{\mathrm{f}}, 0),\\
P_{\mathrm{f}} &= F_{\mathrm{f}}/D_{\mathrm{f}}, \quad F_{\mathrm{f}} = (A\vec{u}\cdot\vec{n})_{\mathrm{f}},\\
D_{\mathrm{f}} &= |\vec{\Delta}|_{\mathrm{f}}(A\Gamma_\varphi)_{\mathrm{f}}/d_{\mathrm{PG}},\\
b_{\mathrm{P}} &= \sum_{\mathrm{f}}(A\Gamma_\varphi)_{\mathrm{f}}(\nabla\varphi)_{\mathrm{f}} \cdot \vec{k}_{\mathrm{f}} + \int_\Omega S_\varphi \mathrm{d}\Omega - \sum_{\mathrm{f}} F_{\mathrm{f}}^H,
\end{aligned}$$

in which $\varphi_{\mathrm{P}}^{\mathrm{O}}$ = value at present time step, φ_{P} = value at next time step. The values of $A(|P|)$, ω_f and F_{f}^H are shown in Table 1.

3.5 *Pressure-correction equation*

The pressure correction equation is derived from the continuity equation in standard pressure correction procedures (Pantankar 1980), and the interface velocity correction is calculated by momentum interpolation methods (Rhie and Chow 1983) to suppress pressure and velocity oscillations (e.g. Neyshabouri *et al.* 2003, Wormleaton and Ewunetu 2006). The coefficient α_p for pressure is also applied. Thus, pressure and velocity are corrected as

$$\begin{aligned}
&a_{\mathrm{P}}p'_{\mathrm{P}} - \sum_{\mathrm{f}} a_{nb}p'_{nb} = b_\varphi\\
&p = p^* + \alpha_p p'\\
&\vec{u} = \vec{u}^* + \vec{u}' = \vec{u}^* - \left(\int_\Omega \nabla p' \mathrm{d}\Omega|_{\mathrm{P}}\right)\Big/ a_{\mathrm{f}}\\
&\quad = \vec{u}^* - \sum_{\mathrm{f}} A_{\mathrm{f}}p'_{\mathrm{f}}\vec{n}
\end{aligned} \quad (13)$$

where

$$\begin{aligned}
a_{\mathrm{P}} &= \sum_{\mathrm{f}} a_{nb}, \quad a_{nb} = A_{\mathrm{f}}\Omega|\vec{\Delta}|/(a_{\mathrm{f}}d_{\mathrm{PG}}),\\
b_\varphi &= -\sum_{\mathrm{f}} F_{\mathrm{f}}^* - \sum_{\mathrm{f}} \Omega A_{\mathrm{f}}\overline{\nabla p'_{\mathrm{f}}} \cdot \vec{k}_{\mathrm{f}}/a_{\mathrm{f}},\\
F_{\mathrm{f}}^* &= (A\vec{u}^* \cdot \vec{n})_{\mathrm{f}}, \quad \overline{\nabla p'_{\mathrm{f}}} = f_{\mathrm{P}}\nabla p'_{\mathrm{P}} + (1 - f_{\mathrm{P}})\nabla p'_{\mathrm{G}}
\end{aligned}$$

Table 1 Values of $A(|P|)$, ω_f and F_{f}^H

Scheme	$A(\|P\|)$	ω_f	F_{f}^H
Q-QUICK	1	0.5	$\max(F_{\mathrm{f}}, 0)(\varphi_{\mathrm{f}})_H^{\max} + \min(F_{\mathrm{f}}, 0)(\varphi_{\mathrm{f}})_H^{\min}$
CDS	1	1	$F_{\mathrm{f}}\nabla\varphi_{\mathrm{f}} \cdot \vec{r}_{\mathrm{IJ}} + \min(F_{\mathrm{f}}, 0)\varphi_{\mathrm{P}}$
UDS	1	0.5	
HDS	$\max(0, 1 - 0.5\|P\|)$	0.5	
PDS	$\max(0, (1 - 0.1\|P\|)^5)$	0.5	

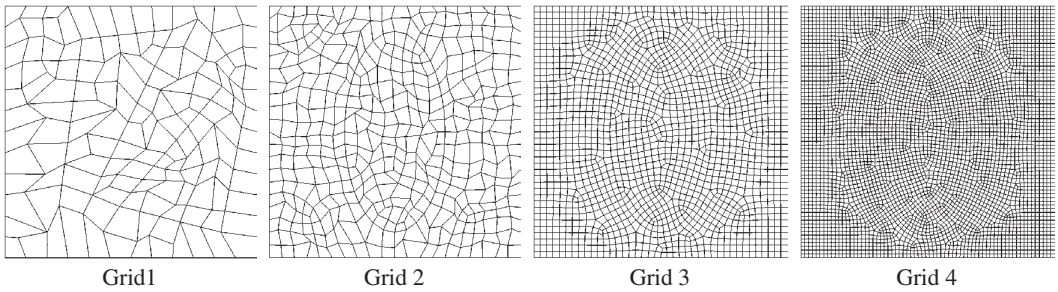

Figure 3 Four different unstructured grids

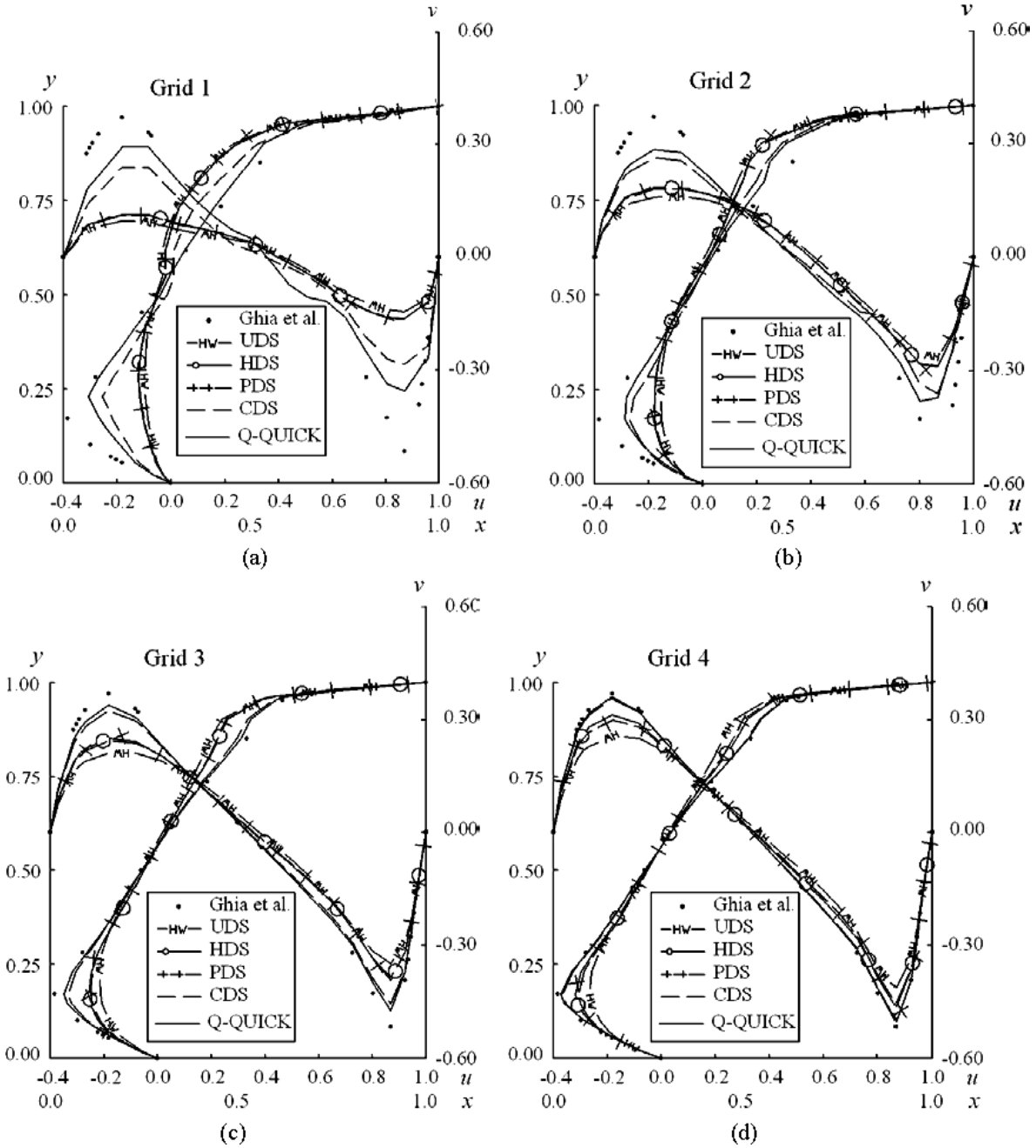

Figure 4 Comparisons of u and v components along vertical and horizontal centerlines under each scheme and unstructured grid for Grids 1 to 4

p' = pressure correction, p^* = pressure at present time, $\vec{u}^*$ = velocity solved from momentum equations using p^*, $\vec{u}'$ = velocity correction, $1/a_f = f_P/a_P + (1 - f_P)/a_G$. In general, the second term of b_φ can be omitted without an effect on the final computational result. Herein, the under-relaxation coefficients are fixed to 0.6 for momentum and 0.4 for pressure-correction for all test cases.

4 Numerical scheme verification

4.1 *90° 2D lid-driven cavity flow*

A standard numerical benchmark of square lid-driven cavity flow with Reynolds number of 1000 (Ghia *et al.* 1982) was selected for the Q-QUICK scheme verification. A grid-dependence study was performed with quadric-lateral grids. These grids include four unstructured mesh numbers, namely 144, 409, 1631 and 4503. The computational grid 1 and grid 2 are intentionally twisted randomly (Fig. 3). The mesh skew angle and the edge ratio are introduced to show the angle between two adjacent sides and the length ratio of the longest and shortest sides of the unstructured grids, respectively. For grid 1, the maximum and minimum mesh skew angles are 174° and 24°, respectively, and the worst edge ratio is 3.49. For grid 2, the maximum and minimum mesh skew angles are 175° and 38°, respectively, with the worst edge ratio of 2.84. To present the numerical performances of Q-QUICK, the schemes UDS/CDS/HDS/PDS were also considered for a comprehensive comparison including the velocity profiles, convergence speed of momentum equation and CPU time consumptions. The Generalized Minimum Residual method (GMRES) (Saad and Schultz 1986) with the incomplete LU precondition was used to accelerate the convergence of the linear equation.

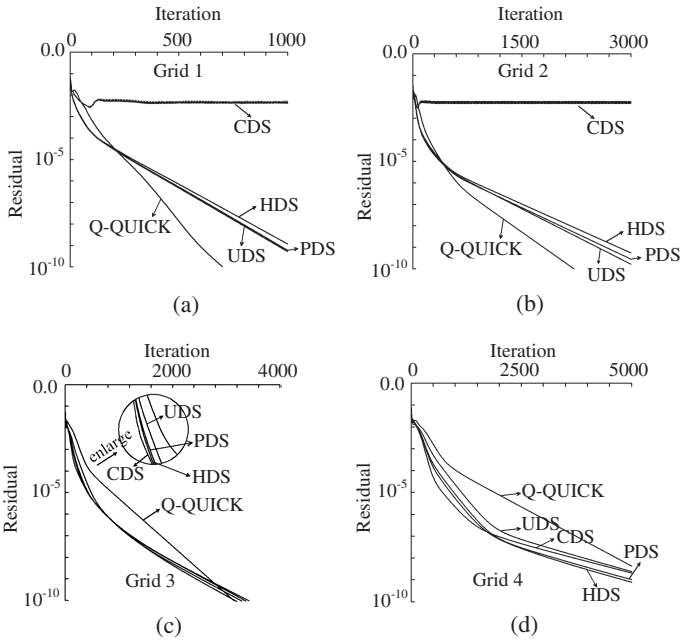

Figure 5 Convergence curves of u momentum equation under each scheme and unstructured grid for Grid (a) 1, (b) 2, (c) 3, (d) 4

A comparison of computational velocity components u along the vertical centerline and v along the horizontal centerline under each scheme and each grid type are shown in Fig. 4. The accuracy

Table 2 Statistic results of numerical performances

Grid type	Scheme	Iterative number	CPU time	Residual of momentum equation	Convergent state
Grid 1	UDS	1000	8.53	5.12E-10	+
	CDS	1000	9.37	4.33E-03	–
	HDS	1000	7.18	1.15E-09	+
	PDS	1000	7.81	5.88E-10	+
	Q-QUICK	739	5.56	1.00E-10	+
Grid 2	UDS	3000	76.43	1.64E-10	+
	CDS	3000	87.20	4.91E-03	–
	HDS	3000	71.16	5.49E-10	+
	PDS	3000	74.11	2.83E-10	+
	Q-QUICK	2220	57.42	1.00E-10	+
Grid 3	UDS	3368	382.20	1.00E-10	+
	CDS	3421	419.50	1.00E-10	+
	HDS	3199	343.72	1.00E-10	+
	PDS	3295	367.02	1.00E-10	+
	Q-QUICK	3141	366.56	1.00E-10	+
Grid 4	UDS	5000	2123.26	2.41E-09	+
	CDS	5000	2151.89	2.06E-09	+
	HDS	5000	2053.61	7.78E-10	+
	PDS	5000	2100.80	1.03E-09	+
	Q-QUICK	5000	2204.23	2.41E-09	+

Note: "+" convergence, "−" divergence.

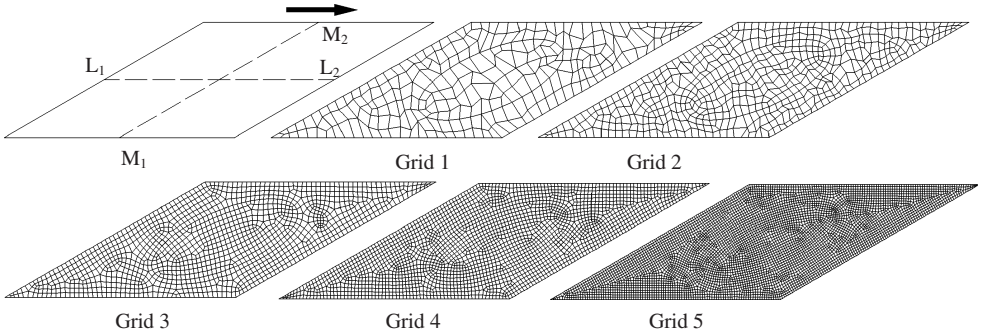

Figure 6 Five different unstructured grids

of Q-QUICK compared with the benchmarks is highest among the schemes considered. Q-QUICK fits well to the benchmarks, even with a relative coarse grid. The convergence curves of the u component are shown in Fig. 5 for each scheme and grid type. The CPU time (Pentium 4 2.4G, 1G memory) consumed by each scheme under each grid type is stated in Table 2. The consumption of CPU time by Q-QUICK is observed to be similar as for the other schemes if fixed iterative numbers are set.

4.2 *30° skew 2D lid-driven cavity flow*

Next, 30° skew lid-driven cavity flow with Reynolds number of 1000 was considered. The present grid-dependence study was carried using five different density grids on unstructured meshes. The mesh numbers, from left to right, are 260, 553, 1245, 2243 and 4991 (Fig. 6). Similarly to Case 1, grid 1 and grid 2 were also intentionally twisted. The maximum and minimum

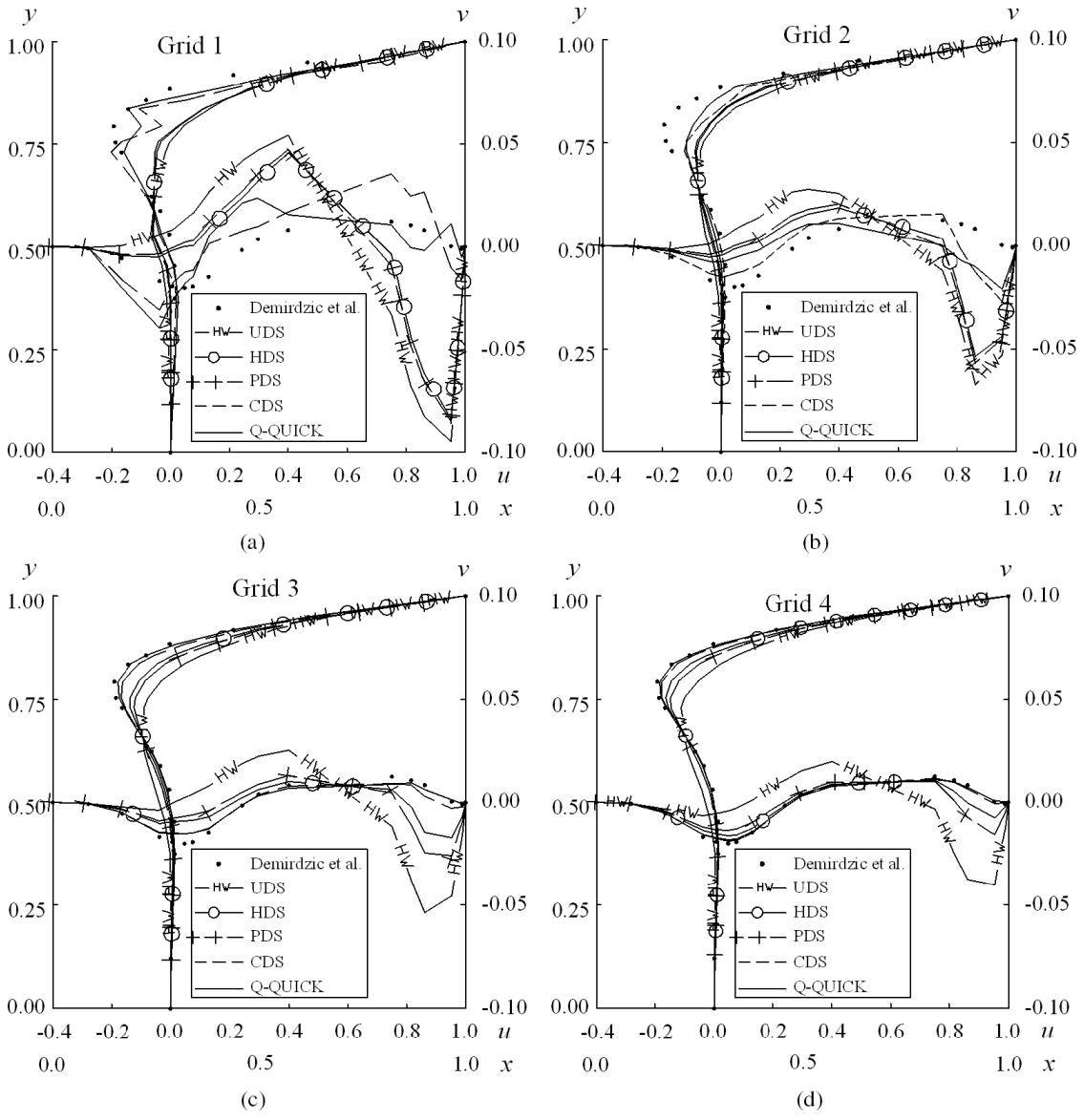

Figure 7 Comparisons of velocities u and v along vertical and horizontal centerlines for Grid (a) 1, (b) 2, (c) 3, (d) 4, (e) 5

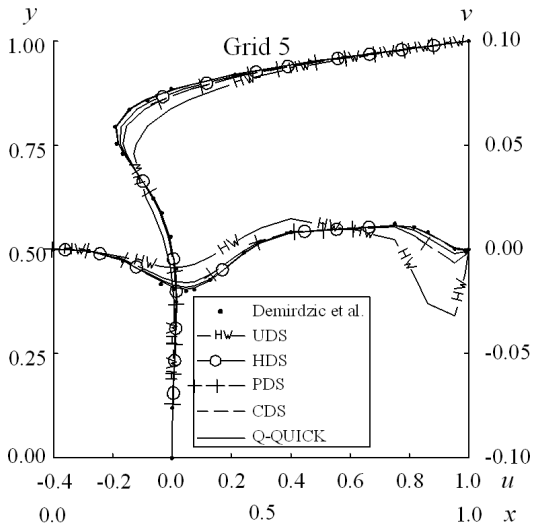

(e)

Figure 7 (*Continued*)

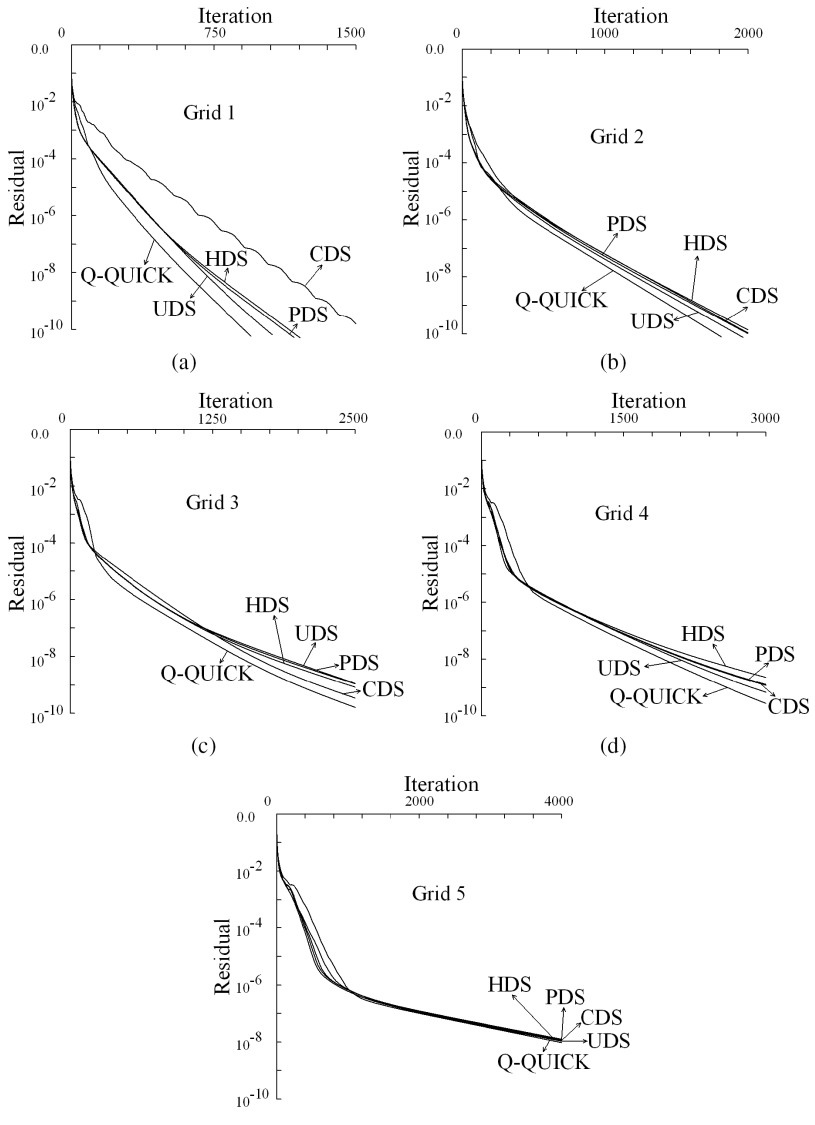

Figure 8 Convergence curves of u for Grid (a) 1, (b) 2, (c) 3, (d) 4, (e) 5

mesh skew angles are 172° and 30° for grid 1, and 170° and 30° for grid 2, respectively. The worst edge ratios are 3.26 for grid 1 and 3.19 for grid 2. The numerical benchmark of Demirdzic *et al*. (1992) was adopted for comparing the schemes. The computational velocity components u and v for each scheme and grid type are shown in Fig. 7. Q-QUICK has an accuracy similar to Case 1. The convergence curves of u are shown in Fig. 8. The convergence speed of Q-QUICK ranks first though with a slow speed at the start of the iterative stage. In addition, the CPU time consumed by each scheme under each grid type is also listed in Table 3. The similar regularities of CPU time consumption are conformed while compared with Case 1.

4.3 *Diverging channel*

A diverging channel was selected to present the behavior of Q-QUICK for relatively coarse and fine grids, using the numerical benchmarks of Napolitano *et al*. (1985) for comparison. The computational domain is shown in Fig. 9(a) and (b), with the inlet at left, and the outlet at right. The upper boundary is a symmetry line, while the lower boundary is a wall specified as

$$y = 5[\tanh(2 - 30x)/\mathsf{R} - \tanh(2)] \tag{14}$$

with $\mathsf{R} = 10$, $0 < x < 3.5$ and inlet velocities

$$u = 3(y - 0.5y^2), \quad v = 0 \tag{15}$$

The interior is filled with coarse and fine quadrangular grids. Each grid type predicts wall vorticity fairly well if the Q-QUICK scheme is employed (Fig. 9c). Almost identical vorticity contours over the whole domain are shown in Fig. 9(d) and (e) for coarse and fine grids, respectively. The good predictions for coarse grids are mainly due to application of the high order scheme Q-QUICK.

This case was also considered using the triangular grids of Davidson (1996). The coarse and fine grids are shown in Fig. 10(a) and (b). Fig. 10(c) compares wall vorticity of the benchmark, the results of Davidson (1996) and Q-QUICK. Note that the curves of Q-QUICK are slightly better fitted to the benchmarks (Napolitano *et al*. 1985). The pressure contours of Q-QUICK and from Davidson (1996) on coarse and fine grids are shown in Fig. 10(d) to (g), respectively.

4.4 *3D lid-driven cavity flow*

Finally, 3D lid-driven cavity flow was chosen for verification, using a unit cubic cavity divided by several parts (Fig. 11a). The computation for $\mathsf{R} = 1000$ was compared with previous numerical solutions of Ku *et al*. (1987), Kato *et al*. (1990), Cortes and Miller (1994), and Babu and Korpela (1994). A group of hybrid grids composed of tetrahedrons, pyramids and hexahedrons is shown in Fig. 11(b) to (d) for the grid-dependence study, and total cells used from grid 1 to grid 3 were 13,042, 29,689 and 62,110, respectively. Correspondingly, the minimum mesh skew

Table 3 Statistic results of numerical performances

Grid type	Scheme	Iterative number	CPU time	Residual of momentum equation	Convergent state
	UDS	1058	14.94	1.00E-10	+
	CDS	1500	21.54	1.57E-10	+
Grid 1	HDS	1208	15.50	1.00E-10	+
	PDS	1173	16.91	1.00E-10	+
	Q-QUICK	946	15.72	1.00E-10	+
	UDS	1972	56.64	1.00E-10	+
	CDS	2000	58.80	1.06E-10	+
Grid 2	HDS	2000	56.08	1.37E-10	+
	PDS	2000	56.86	1.00E-10	+
	Q-QUICK	1814	52.06	1.00E-10	+
	UDS	2500	192.29	1.12E-09	+
	CDS	2500	195.15	3.41E-10	+
Grid 3	HDS	2500	189.97	8.24E-10	+
	PDS	2500	191.63	1.09E-10	+
	Q-QUICK	2500	195.66	1.60E-10	+
	UDS	3000	488.74	6.84E-10	+
	CDS	3000	494.31	1.20E-09	+
Grid 4	HDS	3000	483.95	2.28E-09	+
	PDS	3000	493.32	1.29E-09	+
	Q-QUICK	3000	491.17	2.78E-10	+
	HDS	4000	1911.66	1.26E-08	+
	PDS	4000	1910.73	1.21E-08	+
Grid5	UDS	4000	1914.93	1.07E-08	+
	CDS	4000	1914.41	1.13E-08	+
	Q-QUICK	4000	1940.16	9.57E-09	+

Note: "+" convergence, "−" divergence.

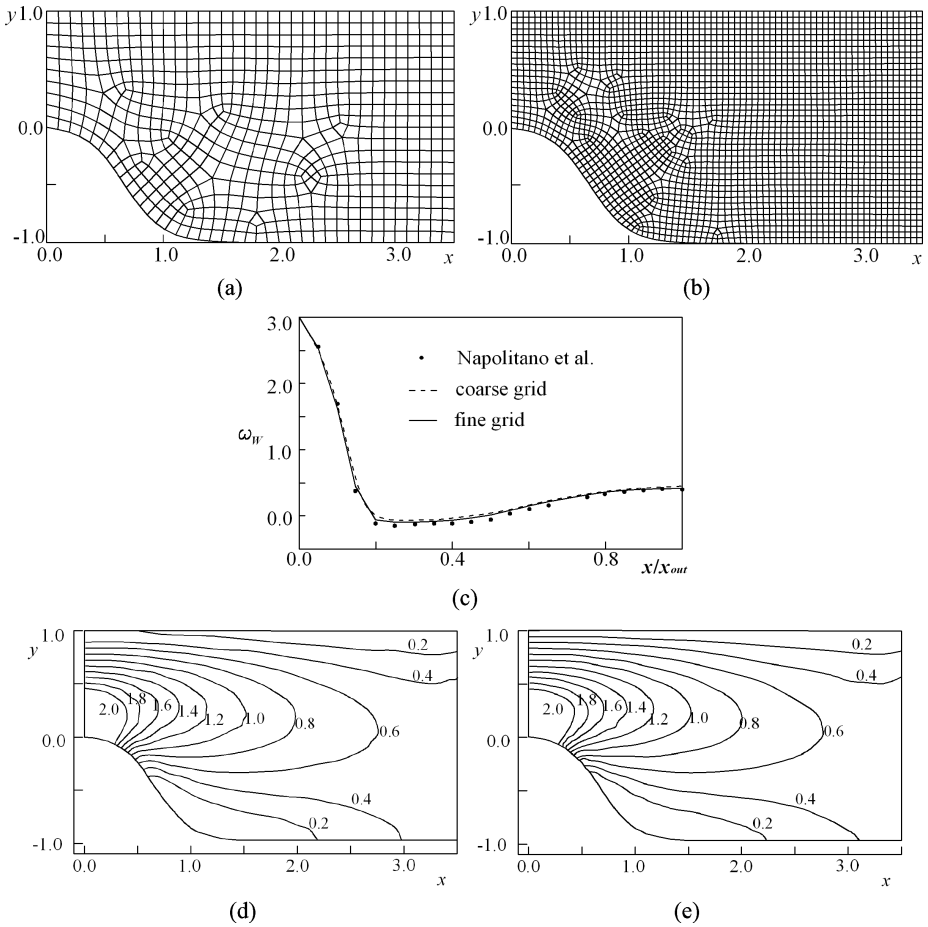

Figure 9 Diverging channel with quadrangular grid (a) coarse grid, (b) fine grid, (c) wall vorticity ω_W, vorticity contours for (d) coarse grid and (e) fine grid

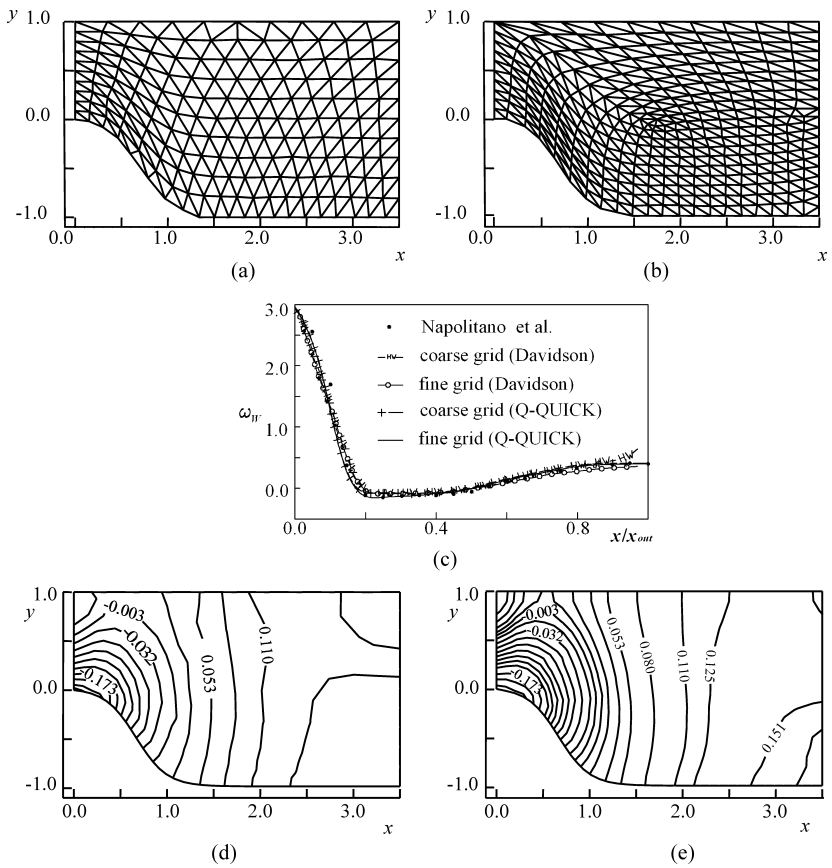

Figure 10 Diverging channel with triangular grid (a) coarse grid, (b) fine grid, (c) wall vorticity ω_W, pressure contours using Q-QUICK for (d) coarse grid, (e) fine grid, pressure contours based on Davidson (1996) for (f) coarse grid (g) fine grid

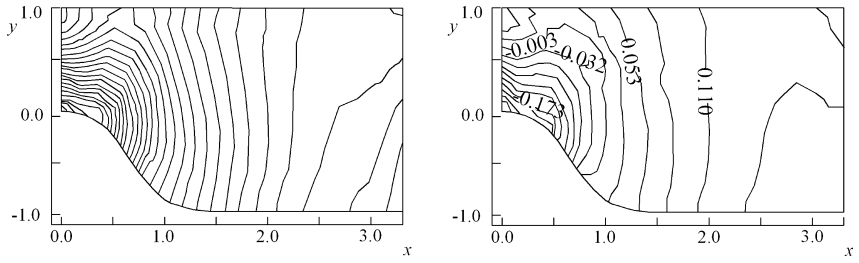

(f) (g)

Figure 10 (*Continued*)

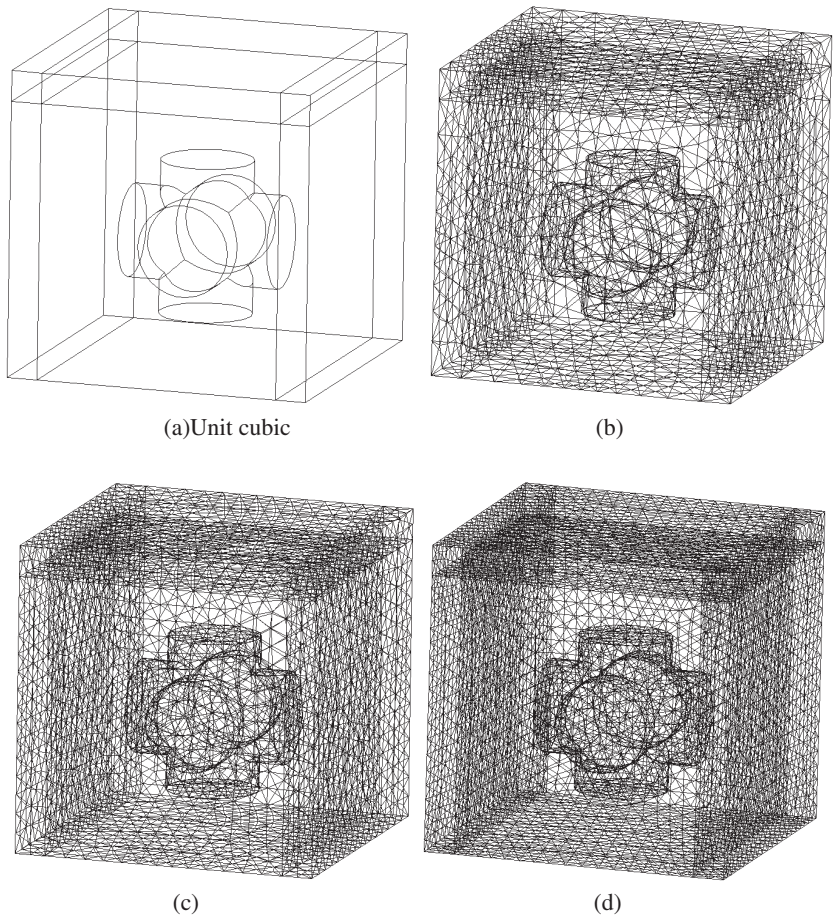

(a)Unit cubic (b)

(c) (d)

Figure 11 Computational domain for (a) and group of 3D hybrid unstructured grids for (b) Grid 1, (c) Grid 2, (d) Grid 3

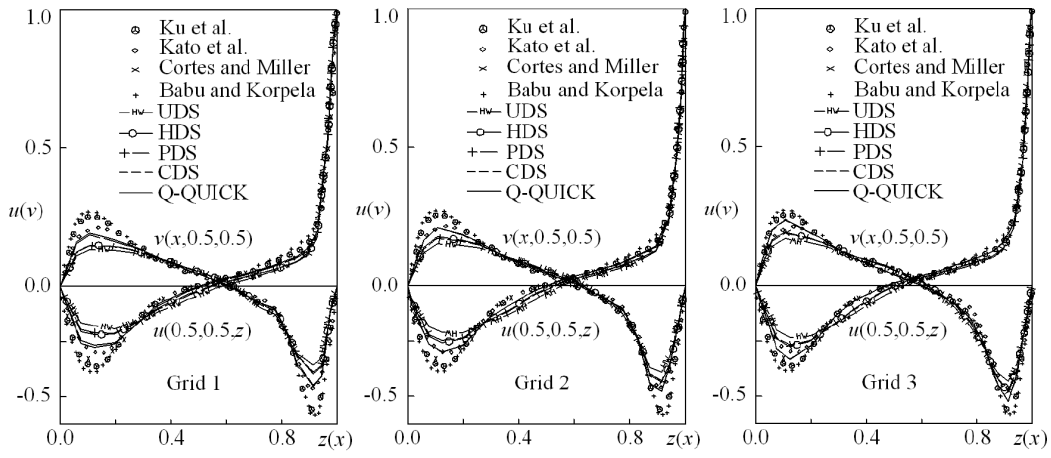

(a) (b) (c)

Figure 12 Comparisons of u and v velocity components along vertical and horizontal centerlines for Grid (a) 1, (b) 2, (c) 3

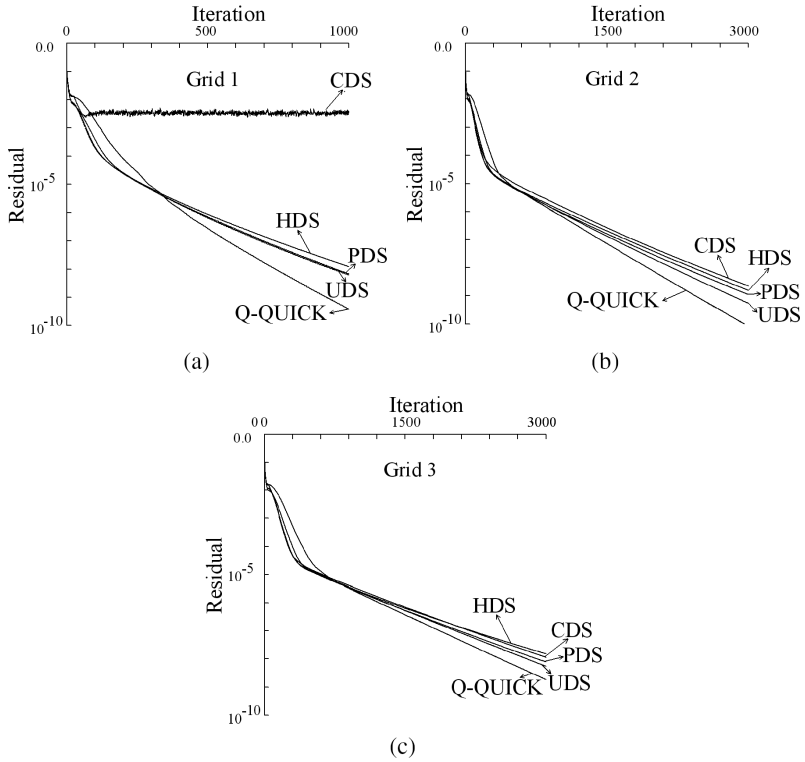

Figure 13 Convergence curves of u for Grid (a) 1, (b) 2, (c) 3

Table 4 Statistic results of numerical performances.

Grid type	Scheme	Iterative number	CPU time	Residual of momentum equation	Convergent state
Grid 1	UDS	1000	1689.4	6.28E-09	+
	CDS	1000	1754.6	3.90E-03	–
	HDS	1000	1756.0	1.21E-08	+
	PDS	1000	1755.0	6.71E-09	+
	Q-QUICK	1000	1540.0	3.76E-10	+
Grid 2	UDS	3000	12814.8	5.48E-09	+
	CDS	3000	13045.2	1.15E-08	+
	HDS	3000	13043.4	1.53E-08	+
	PDS	3000	13100.4	7.81E-09	+
	Q-QUICK	3000	11623.8	1.84E-09	+
Grid 3	UDS	3000	29427.6	5.46E-10	+
	CDS	3000	30167.4	2.24E-09	+
	HDS	3000	29574.0	1.56E-09	+
	PDS	3000	29568.6	1.12E-09	+
	Q-QUICK	3000	26599.8	1.00E-10	+

Note: "+" convergence, "−" divergence

angles are 21.8°, 21.1° and 18.3°. The maximum edge ratios of the tetrahedron, pyramid and hexahedron are 3.3, 2.9 and 6.6, respectively, in grid 1; 6.1, 2.4 and 3.2 in grid 2; and 5.4, 1.9 and 3.8 in grid 3. In Fig. 12, the computational velocity profiles of the u component on the vertical centerline and the v component on the horizontal centerline of plane $y = 0.5$ are shown. The velocities under each numerical scheme and each grid type are compared with other numerical solutions. The accuracy of Q-QUICK is seen to be good. Moreover, Q-QUICK fits well to the previous numerical solutions as the grid numbers increase. The convergence curves of u under each scheme and grid type are shown in Fig. 13. The momentum equation discretized by Q-QUICK converges smoothly for all the three grid types. Additionally, the convergence speed of 3D unstructured grids using Q-QUICK behaves best despite the low speed at the initial iterative stage. Furthermore, the CPU time consumptions under each scheme and each type of grid are also listed in Table 4. Compared with the 2D situations, there are no apparent differences in CPU time consumption while putting aside the magnitude of time itself.

5 Conclusions

In this study, the numerical performance of the Q-QUICK scheme is investigated in terms of numerical accuracy, convergence stability, CPU time consumption and solution sensitivity to high grid deformation. Four cases were considered: 90° and 30° 2D lid-driven cavity flow, diverging channel and 3D lid-driven cavity flow to compare the numerical performances of the scheme Q-QUICK with UDS/CDS/HDS/PDS based on unstructured grids. The main conclusions are:

(1) The accuracy of Q-QUICK is higher as compared with UDS/CDS/HDS/PDS in these test cases. Moreover, small grid numbers are required for Q-QUICK to attain the accuracy requirements as compared with the other schemes. Accordingly, it fits well into the benchmarks as the grid number is increased.
(2) The numerical stability of Q-QUICK is good, even for highly-distorted and -twisted grids. Similar CPU time consumptions are required by Q-QUICK as compared with UDS/CDS/HDS/PDS.
(3) The implementation of Q-QUICK yields good numerical performances in the above test cases. It would be desirable to extend it to much wider applications, such as turbulent transport models or high Reynolds number flows.

Acknowledgements

The research work was partly supported by the National Natural Science Foundation of China (No: 50679019 and 50979026), the National Basic Research Program of China (2008CB418202), the Social Science and Technology Development Project of Jiangsu Province (BS2006095), the 908 Special Foundation of Jiangsu Province (JS-908-02-06) and the Grant of the Changjiang River Scientific Research Institute (YJJ0906/SL01).

Notation

A = Area
d_{PG} = Distance between points P and G
$\vec{n}$ = Outward-pointing face area vector
p = Pressure
p^* = Pressure at present time step
p' = Pressure correction
R = Reynolds number
$\vec{r}_{PU}$ = Distance vector between points P to U
S = Surface of control cell
S_φ = Source term
$\vec{u}$ = Velocity
$\vec{u}^*$ = Velocity solved from momentum equations using values of p^*
$\vec{u}'$ = Velocity correction
u, v = Velocity components
α_p = Under-relaxation coefficient for pressure
α_φ = Under-relaxation coefficient for velocity
δ_1 = Distance between points P and e
δ_2 = Distance between points e and E
Γ_φ = Diffusivity
φ = Typical representative variable
φ_P = Value at next time step
φ_P^O = Value at present time step
ψ_1 = Distance between points W and P
ψ_2 = Distance between points E and EE
Ω = Volume of control cell
ω_W = Wall vorticity

References

Babu, V., Korpela, S.A. (1994). Numerical solutions of the incompressible, three-dimensional Navier-Stokes equations. *Comput. Fluids* 23(5), 675–691.

Basara, B. (2004). Employment of the second-moment turbulence closure on arbitrary unstructured grids. *Int. J. Numer. Meth. Fluids* 44(4), 377–407.

Berour, N., Lacroix, D., Boulet, P., Jeandel, G. (2007). Contribution to the improvement of the QUICK scheme for the resolution of the convection-diffusion problems. *Heat and Mass Transfer* 43, 1075–1085.

Carvalho, R.F., Lemos, C.M., Ramos, C.M. (2008). Numerical computation of the flow in hydraulic jump stilling basins. *J. Hydr. Res.* 46(6), 739–752.

Cortes, A.B., Miller, J.D. (1994). Numerical experiments with the lid-driven cavity flow problem. *Comput. Fluids* 23(8), 1005–1027.

Davidson, L. (1996). A pressure correction method for unstructured meshes with arbitrary control volumes. *Int. J. Numer. Meth. Fluids* 22, 265–281.

Demirdzic, I., Lilek, Z., Peric, M. (1992). Fluid flow and heat transfer test problems for non-orthogonal grids: Bench-mark solutions. *Int. J. Numer. Meth. Fluids* 15(3), 329–354.

Ghia, U., Chia, K.N., Shin, C.T. (1982). High-Re solutions for incompressible flow using Navier-Stokes equations and a multigrid method. *J. Comp. Phys.* 48 (3), 387–411.

Jasak, H. (1996). Error analysis and estimation for the finite volume method with applications to fluid flows. *Ph.D. Thesis*. Imperial College, University of London, London.

Kato, Y., Kawai, H., Tanahashi, T. (1990). Numerical flow analysis in a cubic cavity by the GSMAC finite element method. *Int. J. Series* II JSME 33(4), 649–658.

Ku, H.C., Hirsh, R.S., Taylor, T.D. (1987). A pseudospectral method for solution of the three-dimensional incompressible Navier-Stokes equations. *J. Comput. Phys.* 70(2), 439–462.

Leonard, B.P. (1979). A stable and accurate convective modelling based on quadratic upstream interpolation. *Comp. Meth. Appl. Mech. Engng.* 19, 59–98.

Napolitano, M., Orlando, P. (1985). Laminar flow in complex geometry: a comparison. *Int. J. Numer. Meth. Fluids* 5(8), 667–683.

Neyshabouri, A.A.S., Da Silva, A.M.F., Barron, R. (2003). Numerical simulation of scour by a free falling jet. *J. Hydr. Res.* 41(5), 533–539.

Pantankar, S.V. (1980). *Numerical heat transfer and fluid flow*. McGraw-Hill, New York.

Patel, M.K., Markatos, N.C. (1986). An evaluation of eight discretization schemes for two-dimensional convection-diffusion equations. *Int. J. Numer. Meth. Fluids* 6(3), 129–153.

Pollard, A., Siu, A.L.W. (1982). The calculation of some laminar flows using various discretization schemes. *Comp. Meth. Appl. Mech. Engng.* 35, 293–313.

Rhie, C.M., Chow, W.L. (1983). Numerical study of the turbulent flow past an airfoil with trailing edge separation. *AIAA J.* 21(11), 1525–1532.

Saad, Y., Schultz, M.H. (1986). GMRES, a generalized minimal residual algorithm for solving nonsymmetric linear systems. *SIAM J. Sci. Stat. Comput.* 7(3), 856–869.

Spalding, D.B. (1972). A novel finite difference formulation for differential expressions involving both first and second derivatives. *Int. J. Numer. Meth. Engng.* 4(4), 551–559.

Stamou, A.I., Chapsas, D.G., Christodoulou, G.C. (2008). 3-D numerical modeling of supercritical flow in gradual expansions. *J. Hydr. Res.* 46(3), 402–409.

Tsui Y.Y., Pan Y.F. (2006). A pressure-correction method for incompressible flows using unstructured meshes. *Num. Heat Transfer* B: Fundamentals 49(1), 43–65.

Wei, J.J., Yu, B., Wang, H.S., Tao, W.Q. (2002). Numerical study of simultaneous natural convection heat transfer from both surfaces of a uniformly heated thin plate with arbitrary inclination. *Heat and Mass Transfer* 38(4–5), 309–317.

Wormleaton, P.R., Ewunetu, M. (2006). Three-dimensional k-ε numerical modeling of overbank flow in mobile bed meandering channel with floodplains of different depth, roughness and planform. *J. Hydr. Res.* 44(1), 18–32.